DEPT. OF MATH., UNIVERSITY OF OSLO
RESEARCH REPORT IN MECHANICS, No. 1
ISSN 0801-9940 February 2013

POST-BUCKLING AND ULTIMATE STRENGTH PREDICTION OF COMPOSITE PLATES USING A SEMI-ANALYTICAL METHOD

by

Qiao Jie Yang

Mechanics Division, Department of Mathematics,
University of Oslo

Abstract: The aim of the present work is to predict the ultimate strength of simply supported plates subjected to in-plane compressive load using a semi-analytical method. Based on large deflection theory in combination with first order shear deformation theory, two degradation models have been developed. In the simplest model, at any position in a ply, which has exceeded the given stress criterion, the corresponding stiffness properties are instantaneously degraded throughout that ply. In a slightly more detailed model, the instantaneous material degradation is only applied to the affected regions of a failed ply. For thin plates, there is remarkable improvement by using the more detailed model, while for thick plates the differences are quite insignificant. To give a more accurate estimation of the ultimate stresses, it is necessary to implement a linear material degradation model.

Key words: Composite structures, Plates, Ultimate strength, Post-buckling, Hashin failure criterion, Instantaneous material degradation.

CONTENTS

1 INTRODUCTION

1.1 Background

Plates made of fibre-reinforced composites are widely used in many structures, for example wind turbine blades and ships. In design of such structural elements, to avoid large and significant damages due to regularly acting forces, buckling and ultimate strength are important issues. Finite element (FE) analysis will normally be used in such cases. But these analyses tend to be complex and time consuming to prepare, perform and post-process. Lately, as an alternative to the FE analysis, semi-analytical approaches for buckling and strength analysis have become more common and practical due to their user-friendliness and computational efficiency. The approaches are often tailor-made for specific cases for certain load and boundary conditions, thus they are not so general as FE method. Previously, to estimate the ultimate strength of stiffened and unstiffened thin steel plates under in-plane compression, Steen [1], Brubak *et al.* [2], Brubak and Hellesland [3,4,5,6] have developed several simplified semi-analytical methods. It is desired to extend these methods to fibre-reinforced composite plates having a range of thicknesses.

1.2 The present study

The present paper concerns the prediction of the ultimate strength of composite plates in compression using a semi-analytical method. As a first step to establish a more accurate, simplified and reliable method, several models based on small deflection theory have been presented in [7]. For thicker plates, the results showed reasonable, but somewhat conservative estimations of ultimate strength. For thinner plates, neglect of post-buckling behaviour makes the results very conservative. As an extension of the previous work, the present method is able to take account of:

- failure and degradation models for composites,
- initial geometric imperfections,
- out-of-plane shear deformations which are most relevant for thick composite and sandwich plates, and
- post-buckling deformations, thus the reserve strength of plates which is especially important for thin plates.

Two different degradation approaches in combination with the Hashin failure criterion [8] from 1973 have been developed:

- Complete ply degradation model (CPDM): The material degradation is applied on ply level.
- Ply region degradation model (PRDM): The stiffness degradation is limited to the affected regions of a failed ply.

For both approaches, an energy solution is performed using assumed deformations in the form of a truncated double Fourier series. Further, to validate the method, the results are compared with the FE analysis performed by Misirlis using ABAQUS, and this is reported by Hayman *et al.* [9].

2 LARGE DEFLECTION PLATE THEORY

2.1 Introduction

In order to describe the post-buckling behaviour, the classical large deflection theory (assumptions of moderate rotations, but small in-plane strains) combined with the first order shear deformation theory have been used.

2.2 Kinematics

Based on the classical large deflection theory, the nonlinear strains including the initial imperfections are defined by [10,11]:

$$\varepsilon_{xx} = \varepsilon_{xx}^0 + z\kappa_{xx} = \left(\frac{\partial u_0}{\partial x} + \frac{1}{2}\left(\frac{\partial w}{\partial x} \right)^2 + \frac{\partial w}{\partial x}\frac{\partial w_{init}}{\partial x} \right) + z\left(\frac{\partial \phi_x}{\partial x} \right) \tag{1a}$$

$$\varepsilon_{yy} = \varepsilon_{yy}^0 + z\kappa_{yy} = \left(\frac{\partial v_0}{\partial y} + \frac{1}{2}\left(\frac{\partial w}{\partial y} \right)^2 + \frac{\partial w}{\partial y}\frac{\partial w_{init}}{\partial y} \right) + z\left(\frac{\partial \phi_y}{\partial y} \right) \tag{1b}$$

$$\gamma_{xy} = \gamma_{xy}^0 + z\kappa_{xy} = \left(\frac{\partial u_0}{\partial y} + \frac{\partial v_0}{\partial x} + \frac{\partial w}{\partial x}\frac{\partial w}{\partial y} + \frac{\partial w}{\partial x}\frac{\partial w_{init}}{\partial y} + \frac{\partial w}{\partial y}\frac{\partial w_{init}}{\partial x} \right) + z\left(\frac{\partial \phi_x}{\partial y} + \frac{\partial \phi_y}{\partial x} \right) \tag{1c}$$

$$\gamma_{xz} = \frac{\partial w}{\partial x} + \phi_x \tag{1d}$$

$$\gamma_{yz} = \frac{\partial w}{\partial y} + \phi_y \tag{1e}$$

The terms with the super index "0" denote the mid-plane membrane strains, while κ are the flexural (bending) strains, known as the curvatures. Further, u_0 and v_0 are the mid-plane displacement fields in the x- and y-direction, respectively. The out-of-plane displacement is given by w, and w_{init} is an initial out-of-plane imperfection. Further, z is a distance from the middle plane of the plate. The rotations of a transverse normal about axes parallel to the y and x axes are given by ϕ_x and ϕ_y.

2.3 Material law

For a two-dimensional stress state, the stresses σ_x, σ_y and τ_{xy} in an arbitrary ply are given by [12]:

$$\begin{Bmatrix} \sigma_{xx} \\ \sigma_{yy} \\ \tau_{xy} \end{Bmatrix}_i = \begin{bmatrix} \overline{Q}_{11} & \overline{Q}_{12} & \overline{Q}_{16} \\ \overline{Q}_{21} & \overline{Q}_{22} & \overline{Q}_{26} \\ \overline{Q}_{16} & \overline{Q}_{26} & \overline{Q}_{66} \end{bmatrix} \begin{Bmatrix} \varepsilon_{xx}^0 \\ \varepsilon_{yy}^0 \\ \gamma_{xy}^0 \end{Bmatrix} + z_i \begin{bmatrix} \overline{Q}_{11} & \overline{Q}_{12} & \overline{Q}_{16} \\ \overline{Q}_{21} & \overline{Q}_{22} & \overline{Q}_{26} \\ \overline{Q}_{16} & \overline{Q}_{26} & \overline{Q}_{66} \end{bmatrix} \begin{Bmatrix} \kappa_{xx} \\ \kappa_{yy} \\ \kappa_{xy} \end{Bmatrix} \tag{2}$$

Further, the stresses in the longitudinal (fibre) direction, denoted by subscript 1, the transverse direction, denoted by subscript 2, can be found by

$$\begin{Bmatrix} \sigma_1 \\ \sigma_2 \\ \tau_{12} \end{Bmatrix}_i = [T]_i \begin{Bmatrix} \sigma_{xx} \\ \sigma_{yy} \\ \tau_{xy} \end{Bmatrix} \tag{3}$$

Where $[T]$ is the transformation matrix for ply i.

2.4 Boundary conditions and displacement fields

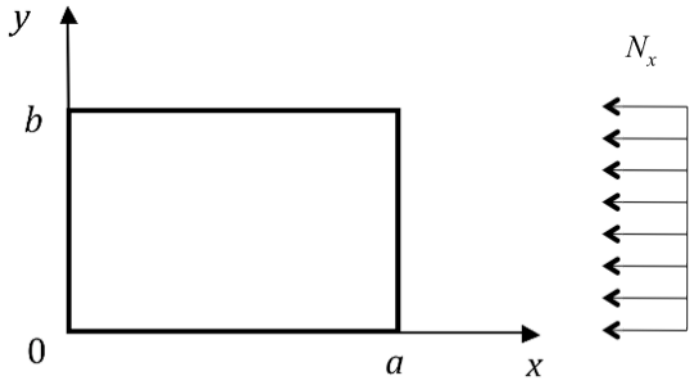

Fig. 1. Plate geometry and load condition.

A plate with dimensions $a \times b$ (Fig. 1) with an initial deformation w_{init} is considered. The plate is simply supported on all edges and subjected to uniform compression N_x in the x-direction. In the analyses, this is achieved by restraining the edge $x = 0$ in the x-direction and applying a mean compressive loading N_x in the x-direction on the edge $x = a$, all edges being held straight. The total out-of-plane deformation is $w_{tot}=w_{init}+w$, where w is an additional deformation because of the load N_x. The following double Fourier series are assumed to represent u, v, ϕ_x, ϕ_y and w_{tot} [6,12]:

$$u_0(x,y) = \sum_{n=1}^{N}\sum_{m=1}^{M} u_{mn} \sin\left(\frac{m\pi x}{a}\right)\sin\left(\frac{n\pi y}{b}\right) + u_c \frac{x}{a} \tag{4a}$$

$$v_0(x,y) = \sum_{n=1}^{N}\sum_{m=1}^{M} v_{mn} \sin\left(\frac{m\pi x}{a}\right)\sin\left(\frac{n\pi y}{b}\right) + v_c \frac{x}{a} \tag{4b}$$

$$\phi_x(x,y) = \sum_{n=1}^{N}\sum_{m=1}^{M} x_{mn} \cos\left(\frac{m\pi x}{a}\right)\sin\left(\frac{n\pi y}{b}\right) \tag{4c}$$

$$\phi_y(x,y) = \sum_{n=1}^{N}\sum_{m=1}^{M} y_{mn} \sin\left(\frac{m\pi x}{a}\right)\cos\left(\frac{n\pi y}{b}\right) \tag{4d}$$

$$\begin{aligned} w_{tot}(x,y) &= w(x,y) + w_{init}(x,y) \\ &= \sum_{n=1}^{N}\sum_{m=1}^{M} w_{mn} \sin\left(\frac{m\pi x}{a}\right)\sin\left(\frac{n\pi y}{b}\right) + \sum_{n=1}^{N}\sum_{m=1}^{M} w_{imn} \sin\left(\frac{m\pi x}{a}\right)\sin\left(\frac{n\pi y}{b}\right) \end{aligned} \tag{4e}$$

Here, u_{mn}, v_{mn}, x_{mn}, y_{mn} and w_{mn} are the unknown series coefficients, while u_c and v_c are

the unknown coefficients in the linear in-plane displacement fields. Further, m, n, M and N are positive integers, and w_{imn} are given imperfection amplitudes.

3 POTENTIAL ENERGY

3.1 Introduction

The total potential energy consists of three contributions associated, respectively, with in-plane strain energy, shear strain energy and external forces:

$$\Pi = U_p + U_s + U_f \tag{5}$$

3.2 Membrane and bending strain energy

The in-plane strain energy can be divided into a membrane contribution and a bending contribution, and then U_p can be written as

$$\begin{aligned} U_p &= \frac{1}{2}\int_V \varepsilon_p^T \sigma_p \, dV = \frac{1}{2}\int_A \int_{-h/2}^{h/2} \varepsilon_p^T \overline{Q} \varepsilon_p \, dz \, dA \\ &= \frac{1}{2}\int_A \left(\left(\varepsilon^0\right)^T A \varepsilon^0 + 2\left(\varepsilon^0\right)^T B\kappa + \kappa^T D\kappa \right) dA \\ &= U_m + U_{mb} + U_b \end{aligned} \tag{6}$$

where U_m and U_b are the potential membrane and bending strain energy, respectively. U_{mb} gives the potential strain energy due to the coupling terms between the membrane and bending contributions.

$$\begin{aligned} U_m = \frac{1}{2}\int_A \left(\varepsilon^0\right)^T A\varepsilon^0 dA = \frac{1}{2}\int_0^b \int_0^a & A_{11}\left(\varepsilon_{xx}^0\right)^2 + 2A_{12}\varepsilon_{xx}^0\varepsilon_{yy}^0 + A_{22}\left(\varepsilon_{yy}^0\right)^2 \\ & + 2A_{16}\varepsilon_{xx}^0\gamma_{xy}^0 + 2A_{26}\varepsilon_{yy}^0\gamma_{xy}^0 + A_{66}\left(\gamma_{xy}^0\right)^2 dxdy \end{aligned} \tag{7a}$$

$$\begin{aligned} U_{mb} = \frac{1}{2}\int_A 2\left(\varepsilon^0\right)^T B\kappa dA = \frac{1}{2}\int_0^b \int_0^a & B_{11}\varepsilon_{xx}^0\kappa_{xx} + B_{12}\left(\varepsilon_{xx}^0\kappa_{yy} + \varepsilon_{yy}^0\kappa_{xx}\right) + B_{22}\varepsilon_{yy}^0\kappa_{yy} \\ & + B_{16}\left(\varepsilon_{xx}^0\kappa_{xy} + \gamma_{xy}^0\kappa_{xx}\right) + B_{26}\left(\varepsilon_{yy}^0\kappa_{xy} + \gamma_{xy}^0\kappa_{yy}\right) + B_{66}\gamma_{xy}^0\kappa_{xy} dxdy \end{aligned} \tag{7b}$$

$$\begin{aligned} U_b = \frac{1}{2}\int_A \kappa^T D\kappa dA = \frac{1}{2}\int_0^b \int_0^a & D_{11}\left(\kappa_{xx}\right)^2 + 2D_{12}\kappa_{xx}\kappa_{yy} + D_{22}\left(\kappa_{yy}\right)^2 \\ & + 2D_{16}\kappa_{xx}\kappa_{xy} + 2D_{26}\kappa_{yy}\kappa_{xy} + D_{66}\left(\kappa_{xy}\right)^2 dxdy \end{aligned} \tag{7c}$$

The extensional stiffness matrix is given by A_{ij}, while B_{ij} and D_{ij} are the bending-stretching coupling matrix and the bending stiffness matrix, respectively.

3.3 Shear strain energy

The potential energy due to shear strain is given in equation (8):

$$U_s = \frac{1}{2}\int_V \varepsilon_s^T \sigma_s dV = \frac{1}{2}\int_A \int_{-h/2}^{h/2} \varepsilon_s^T \overline{Q}_s \varepsilon_s \, dz\, dA = \frac{1}{2}\int_A \varepsilon_s^T A_s \varepsilon_s dA$$
$$= \frac{1}{2} k \int_0^b \int_0^a A_{44}\left(\phi_y + \frac{\partial w}{\partial y}\right)^2 + A_{55}\left(\phi_x + \frac{\partial w}{\partial x}\right)^2 dxdy \tag{8}$$

Here, A_{ij} ($i = j = 4, 5$) is the stiffness matrix for transverse shear and k (= 5/6) is the shear correction coefficient.

3.4 External forces

The potential energy of an external, in-plane load N_x in the x-direction is given by

$$U_f = \Lambda N_x b u_c \tag{9}$$

where Λ is a load parameter, b is the width of the plate and u_c is the plate shortening in the x-direction.

4 SOLUTION PROCEDURE

4.1 Incremental response propagation

The post-buckling response is traced by an incremental procedure [1]. Here, an arc length parameter is used as a propagation parameter.

Using large deflection theory, the equilibrium equations obtained from the Rayleigh-Ritz method are nonlinear. Instead of solving the nonlinear equations directly, these are solved incrementally by computing the rate form of the equilibrium equations with respect to an arc length parameter η. Further, the change in the arc length parameter is associated with a change in the external stresses and the displacements/rotations. This relationship can be illustrated graphically (Fig. 2).

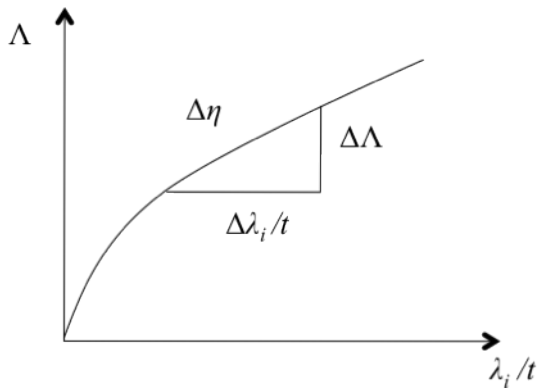

Fig. 2. Relationship between an arc length parameter increment $\Delta\eta$, a load increment $\Delta\Lambda$ and an incremental displacement/roration amplitude $\Delta\lambda_i$.

As the increment size approaches zero, the relationship can be given by

$$
\begin{aligned}
&(\Delta\Lambda)^2 + \left(\frac{\Delta\lambda_i}{t}\right)^2 = (\Delta\eta)^2 \\
\Rightarrow &\left(\frac{\Delta\Lambda}{\Delta\eta}\right)^2 + \frac{1}{t^2}\left(\frac{\Delta\lambda_i}{\Delta\eta}\right)^2 = 1 \\
\Rightarrow &\left(\frac{\partial\Lambda}{\partial\eta}\right)^2 + \frac{1}{t^2}\left(\frac{\partial\lambda_i}{\partial\eta}\right)^2 = 1 \\
\Rightarrow &\dot{\Lambda}^2 + \sum_{i=1}^{N_{tot}} \frac{\dot{\lambda}_i^2}{t^2} = 1
\end{aligned}
\tag{10}
$$

Where N_{tot} is the total number of degrees of freedom, while Λ is the load parameter, λ_i represents the displacement and rotation amplitudes and t is the plate thickness. A dot above a symbol can be interpreted as differentiation with respect to the arc length parameter η. From equations (4), the displacement and rotation components are defined by

$$
\begin{aligned}
\left[\lambda_i\right] &= \left[\lambda_1, \lambda_2, ..., \lambda_{N_{tot}}\right] \\
&= \left[u_c, u_{11}, u_{12}, ..., u_{1N}, u_{21}, u_{22}, ..., u_{M1}, u_{M2}, ..., u_{MN},\right. \\
&\quad v_c, v_{11}, v_{12}, ..., v_{1N}, v_{21}, v_{22}, ..., v_{M1}, v_{M2}, ..., v_{MN}, \\
&\quad x_{11}, x_{12}, ..., x_{1N}, x_{21}, x_{22}, ..., x_{M1}, x_{M2}, ..., x_{MN}, \\
&\quad y_{11}, y_{12}, ..., y_{1N}, y_{21}, y_{22}, ..., y_{M1}, y_{M2}, ..., y_{MN}, \\
&\quad \left. w_{11}, w_{12}, ..., w_{1N}, w_{21}, w_{22}, ..., w_{M1}, w_{M2}, ..., w_{MN}\right]
\end{aligned}
\tag{11}
$$

Further, in the incremental procedure, the load parameter Λ and displacement/roration amplitudes λ_i are functions of the arc length parameter η. For an increment $\Delta\eta$ along the equilibrium curve from point s to (s +1), a Taylor series expansion gives

$$
\lambda_i^{s+1} = \lambda_i^s + \dot{\lambda}_i^s \Delta\eta + \frac{1}{2}\ddot{\lambda}_i^s \Delta\eta^2 + ... \tag{12a}
$$

$$
\Lambda^{s+1} = \Lambda^s + \dot{\Lambda}^s \Delta\eta + \frac{1}{2}\ddot{\Lambda}^s \Delta\eta^2 + ... \tag{12b}
$$

The second and higher order terms are neglected in the present work, i.e. the expansion is of first order. In other works, such as in Byklum [13], it is shown how to include the second order terms. However, it is believed that by choosing smaller increment, the results achieved by the first order expansion are satisfactory. Besides, retaining the second or higher order terms, or using equilibrium corrections after each increment such as Riks arc length method [14] to improve the accuracy, is computationally costly and will not likely give significant computational gains.

4.2 Incremental equilibrium equations

The Rayleigh-Ritz method on an incremental form or rate form as mentioned in Section 4.1 has been used to solve the problem. The total potential energy is given by equation (5). Now, equilibrium requires that $\delta\dot{\Pi} = 0$, then

$$\frac{\partial\dot{\Pi}}{\partial\lambda_i} = \frac{\partial}{\partial\eta}\left(\frac{\partial\Pi}{\partial\lambda_i}\right) = \frac{\partial}{\partial\lambda_i}\left(\frac{\partial\Pi}{\partial\eta}\right) = \frac{\partial}{\partial\lambda_i}\left(\frac{\partial\Pi}{\partial\lambda_j}\right)\frac{\partial\lambda_j}{\partial\eta} + \frac{\partial}{\partial\lambda_i}\left(\frac{\partial\Pi}{\partial\Lambda}\right)\frac{\partial\Lambda}{\partial\eta}$$
$$= \frac{\partial^2\Pi}{\partial\lambda_i\partial\lambda_j}\dot{\lambda}_j + \frac{\partial^2\Pi}{\partial\lambda_i\partial\Lambda}\dot{\Lambda} = C_{ij}\dot{\lambda}_j + F_i\dot{\Lambda} = 0 \tag{13}$$

Here, C_{ij} is a generalised, incremental stiffness matrix and $F_i\dot{\Lambda}$ is a generalised, incremental load vector. Further, *i* indicates the row number, while *j* indicates the column number in a matrix. The total number of unknowns are $N_{tot} + 1$ (λ_i and Λ), while there are N_{tot} equations in equation (13). The additional equation required is given by equation (10).

Based on equation (11), equation (13) can be written in matrix form:

$$\begin{bmatrix}
\frac{\partial^2\Pi}{\partial u_c\partial u_c} & \frac{\partial^2\Pi}{\partial u_c\partial v_c} & \frac{\partial^2\Pi}{\partial u_c\partial u_{ij}} & \frac{\partial^2\Pi}{\partial u_c\partial v_{ij}} & \frac{\partial^2\Pi}{\partial u_c\partial x_{ij}} & \frac{\partial^2\Pi}{\partial u_c\partial y_{ij}} & \frac{\partial^2\Pi}{\partial u_c\partial w_{ij}} \\
\frac{\partial^2\Pi}{\partial v_c\partial u_c} & \frac{\partial^2\Pi}{\partial v_c\partial v_c} & \frac{\partial^2\Pi}{\partial v_c\partial u_{ij}} & \frac{\partial^2\Pi}{\partial v_c\partial v_{ij}} & \frac{\partial^2\Pi}{\partial v_c\partial x_{ij}} & \frac{\partial^2\Pi}{\partial v_c\partial y_{ij}} & \frac{\partial^2\Pi}{\partial v_c\partial w_{ij}} \\
\frac{\partial^2\Pi}{\partial u_{fg}\partial u_c} & \frac{\partial^2\Pi}{\partial u_{fg}\partial v_c} & \frac{\partial^2\Pi}{\partial u_{fg}\partial u_{ij}} & \frac{\partial^2\Pi}{\partial u_{fg}\partial v_{ij}} & \frac{\partial^2\Pi}{\partial u_{fg}\partial x_{ij}} & \frac{\partial^2\Pi}{\partial u_{fg}\partial v_{ij}} & \frac{\partial^2\Pi}{\partial u_{fg}\partial w_{ij}} \\
\frac{\partial^2\Pi}{\partial v_{fg}\partial u_c} & \frac{\partial^2\Pi}{\partial v_{fg}\partial v_c} & \frac{\partial^2\Pi}{\partial v_{fg}\partial u_{ij}} & \frac{\partial^2\Pi}{\partial v_{fg}\partial v_{ij}} & \frac{\partial^2\Pi}{\partial v_{fg}\partial x_{ij}} & \frac{\partial^2\Pi}{\partial v_{fg}\partial y_{ij}} & \frac{\partial^2\Pi}{\partial v_{fg}\partial w_{ij}} \\
\frac{\partial^2\Pi}{\partial x_{fg}\partial u_c} & \frac{\partial^2\Pi}{\partial x_{fg}\partial v_c} & \frac{\partial^2\Pi}{\partial x_{fg}\partial u_{ij}} & \frac{\partial^2\Pi}{\partial x_{fg}\partial v_{ij}} & \frac{\partial^2\Pi}{\partial x_{fg}\partial x_{ij}} & \frac{\partial^2\Pi}{\partial x_{fg}\partial y_{ij}} & \frac{\partial^2\Pi}{\partial x_{fg}\partial w_{ij}} \\
\frac{\partial^2\Pi}{\partial y_{fg}\partial u_c} & \frac{\partial^2\Pi}{\partial y_{fg}\partial v_c} & \frac{\partial^2\Pi}{\partial y_{fg}\partial u_{ij}} & \frac{\partial^2\Pi}{\partial y_{fg}\partial v_{ij}} & \frac{\partial^2\Pi}{\partial y_{fg}\partial x_{ij}} & \frac{\partial^2\Pi}{\partial y_{fg}\partial y_{ij}} & \frac{\partial^2\Pi}{\partial y_{fg}\partial w_{ij}} \\
\frac{\partial^2\Pi}{\partial w_{fg}\partial u_c} & \frac{\partial^2\Pi}{\partial w_{fg}\partial v_c} & \frac{\partial^2\Pi}{\partial w_{fg}\partial u_{ij}} & \frac{\partial^2\Pi}{\partial w_{fg}\partial v_{ij}} & \frac{\partial^2\Pi}{\partial w_{fg}\partial x_{ij}} & \frac{\partial^2\Pi}{\partial w_{fg}\partial y_{ij}} & \frac{\partial^2\Pi}{\partial w_{fg}\partial w_{ij}}
\end{bmatrix}$$

$$\cdot\begin{bmatrix} \dot{u}_c \\ \dot{v}_c \\ \dot{u}_{ij} \\ \dot{v}_{ij} \\ \dot{x}_{ij} \\ \dot{y}_{ij} \\ \dot{w}_{ij} \end{bmatrix} + \begin{bmatrix} \dfrac{\partial^2 \Pi}{\partial u_c \partial \Lambda} \\ \dfrac{\partial^2 \Pi}{\partial v_c \partial \Lambda} \\ \dfrac{\partial^2 \Pi}{\partial u_{fg} \partial \Lambda} \\ \dfrac{\partial^2 \Pi}{\partial v_{fg} \partial \Lambda} \\ \dfrac{\partial^2 \Pi}{\partial x_{fg} \partial \Lambda} \\ \dfrac{\partial^2 \Pi}{\partial y_{fg} \partial \Lambda} \\ \dfrac{\partial^2 \Pi}{\partial w_{fg} \partial \Lambda} \end{bmatrix} \cdot \dot{\Lambda} = 0 \tag{14}$$

The row number is indicated by *f* and *g* for corresponding displacement and rotation amplitude with two subscripts. Further, in a similar way, *i* and *j* are used to indicate the column number.

4.3 Procedure for solving the equations

First, $\dot{\lambda}_j$ and $\dot{\Lambda}$ can be found by solving the equations (10) and (13). The solution of equation (13) is given by

$$\dot{\lambda}_j = -\dot{\Lambda} C_{ij}^{-1} F_i \tag{15}$$

Now, substituting equation (15) into equation (10):

$$\dot{\Lambda}^2 \left(t^2 + \sum_{i,j=1}^{N_{tot}} \left(C_{ij}^{-1} F_i \right)^2 \right) = t^2 \tag{16}$$

The load rate parameter $\dot{\Lambda}$ can be determined as

$$\dot{\Lambda} = \pm \frac{t}{\sqrt{t^2 + \sum_{i,j=1}^{N_{tot}} \left(C_{ij}^{-1} F_i \right)^2}} \tag{17}$$

According to equation (17), there are two possible solutions with same numerical values, but opposite signs along the equilibrium curve. For choosing the correct solution, the angle criterion is applicable to use. Based on the assumption that the

equilibrium curve is smooth, it is interested to find the solution giving a continuous increase of the arc length. This is achieved by the requirement that the absolute value of the angle between the tangents of the consecutive increments ($s-1$) and s in the load-displacement/rotation space ($\Lambda - \lambda_j/t$) is smaller than 90°. For the positive sign of the load rate $\dot{\Lambda}^s$ at stage s, the following equivalent criterion must be satisfied [1]:

$$\sum_{i,j=1}^{N_{tot}} \dot{\Lambda}^s \left(\frac{\left(-C_{ij}^{-1} F_i\right)^s \dot{\lambda}_j^{s-1}}{t^2} + \dot{\Lambda}^{s-1} \right) > 0 \tag{18}$$

When $\dot{\Lambda}^s$ at stage s is found, the displacement and rotation rate amplitudes $\dot{\lambda}_j^s$ at the stage s are given by equation (15). The displacement and rotation amplitudes, and load parameter at the next stage are then obtained by the first order Taylor series expansion:

$$\lambda_j^{s+1} = \lambda_j^s + \dot{\lambda}_j^s \Delta\eta \tag{19a}$$

$$\Lambda^{s+1} = \Lambda^s + \dot{\Lambda}^s \Delta\eta \tag{19b}$$

As mentioned in section 4.1, $\Delta\eta$ has to be small to give a satisfactory result. The solution propagation is continued until a given failure criterion is reached.

5 PROGRESSIVE FAILURE MODELS

5.1 Hashin failure criterion

The 1973 Hashin failure criterion for in-plane stresses can be written [8]:

$$f_1^T = \left(\frac{\sigma_1}{X_t} \right)^2 = 1 \tag{20a}$$

$$f_1^C = \left(\frac{\sigma_1}{X_c} \right)^2 = 1 \tag{20b}$$

$$f_2^T = \left(\frac{\sigma_2}{Y_t} \right)^2 + \left(\frac{\tau_{12}}{S_{12}} \right)^2 = 1 \tag{20c}$$

$$f_2^C = \left(\frac{\sigma_2}{Y_c} \right)^2 + \left(\frac{\tau_{12}}{S_{12}} \right)^2 = 1 \tag{20d}$$

Failure occurs when any of the four failure functions from equations (20) reaches unity. Each is associated with a dominant failure mode.

5.2 Degradation of properties

When failure occurs in a laminated composite plate, the effective material properties change. This results in a new stiffness of the plate. To describe this behaviour, a damaged stiffness matrix for in-plane deformations is defined [9]:

$$[R]=\begin{bmatrix} (1-d_1)R_{11} & (1-d_1)(1-d_2)R_{12} & 0 \\ sym. & (1-d_2)R_{22} & 0 \\ sym. & sym. & (1-d_6)R_{66} \end{bmatrix} \tag{21}$$

Here d_1 is the damage factor in the longitudinal direction of the material, d_2 is the damage factor in the transverse direction, and d_6 is the damage factor in the in-plane shear component. The remaining parameters in equation (21) are defined as $R_{11}=\frac{E_1}{\Delta}$, $R_{22}=\frac{E_2}{\Delta}$, $R_{12}=\frac{\nu_{12}E_2}{\Delta}$, $R_{66}=G_{12}$ and $\Delta=1-\nu_{12}\nu_{21}(1-d_1)(1-d_2)$.

For the Hashin criterion, because the shear failure component is associated with the fibre and matrix modes of failure, the damage variable d_6 is defined as:

$$d_6=1-(1-d_1)(1-d_2) \tag{22}$$

The transverse (out-of-plane) shear stiffness matrix is defined in equation (23), and (following Misirlis [9]) is not degraded during the analysis:

$$[K]=\begin{bmatrix} K_{44} & 0 \\ 0 & K_{55} \end{bmatrix} \tag{23}$$

where $K_{44}=G_{23}$ and $K_{55}=G_{13}$.

The instantaneous degradation of material properties is used in the progressive failure model reported here. When any ply or region fulfils a stress criterion, its corresponding properties are instantaneously reduced to a predefined value equal to 1% of the respective initial values [15]. Thus the associated damage factor $d_i = 0.99$. In contrast, Misirlis [9] assumed a linear degradation of the properties [16] in his progressive failure model when using the Hashin criterion. Fig. 3 shows these material degradations mentioned here.

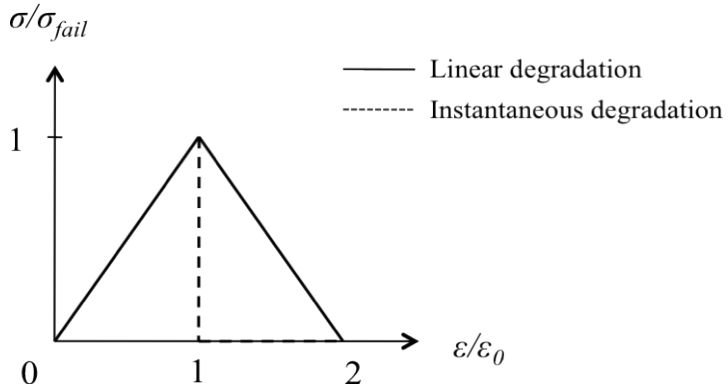

Fig. 3. Material degradations.

6 DEGRADATION MODELS

6.1 Complete ply degradation model (CPDM)

The model presented in this sub-section is based on using the Rayleigh-Ritz method. The boundary condition is given in Section 2.4 with the corresponding displacement field assumed in equations (4). The total potential energy is provided in equation (5) and equations (7)-(9). The unknown coefficients could be found by following the solution procedure described in Section 4.3. In the ply which has exceeded a given stress criterion, the degradation of the corresponding properties is then applied to the entire ply. The load is then applied with the reduced stiffness until either a further criterion is exceeded in the same ply or failure occurs in a different ply. Again, the associated material degradation is applied to the entire ply. The process is repeated until the maximum value of load is reached; this is considered to be the ultimate load.

The more detailed degradation procedure is the following:

- From equations (19), the corresponding displacements, rotations, and load parameter are found for a given value of applied reference load, N_x.
- Then, the in-plane stresses in each ply are calculated using equations (2)-(3).
- The Hashin failure criterion is applied for failure checking.
- Repetition of the previous steps with increasing applied load based on the solution procedure described in Section 4.3. This is continued until first ply failure (FPF) is detected.
- The failure location is determined (both ply number and (x,y)-coordinates).
- In the ply which has exceeded a given stress criterion, the corresponding properties are degraded. The degradation is applied to the entire ply.
- The A-, B- and D-matrices are computed for the degraded plate.
- For a given value of applied load, the corresponding displacements, rotations, load parameter and stresses in each ply are calculated.
- The failure criterion is applied in order to find the load and location at which failure next occurs in the degraded plate. This may involve either a further criterion being exceeded in the same ply as before, or failure occurring in a different ply.
- Again, the appropriate degradation is applied to the entire ply.
- The process is continued until the loading at occurrence of failure reaches its highest value (the ultimate load).

6.2 Ply region degradation model (PRDM)

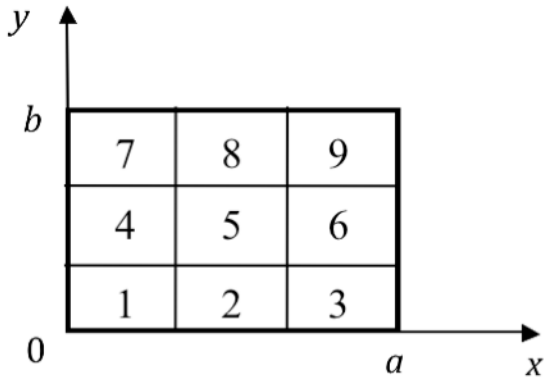

Fig. 4. Plate geometry**.**

The model presented in this sub-section is based on Fig. 4. A plate with dimensions $a \times b$ has been divided into 9 regions. The displacement fields are assumed in equations (4), while the total potential energy is again given by equation (5) and equations (7)-(9). The unknown displacement and rotation amplitudes can be found by solution procedure described in Section 4.3. The progressive failure model with degraded material properties is now implemented by reducing the appropriate terms in the equations (7)-(8) in the specific region of the ply where failure has occurred.

The degradation procedure is similar to that described in Section 6.1, but degradation at each stage is applied only over that region of a ply that has fulfilled the failure criterion as indicated above.

7 RESULTS FROM THE PARAMETRIC STUDY ON SQUARE PLATES

7.1 Geometries and material properties

The parametric studies have been performed for a series of square plates, with $a = b = 500$ mm, having various breadth/thickness (b/t) ratios. The plates are simply supported on all edges and subjected to uniform compression N_x in the x-direction (see Fig. 1, Section 2.4). Three different maximum initial imperfection amplitudes have been examined. They are respectively 0.1%, 1% and 3% of the width b (= 500 mm). The assumed shape of the initial geometric imperfection is a single half sine wave in each direction, so that $w_{imn} = 0$ for all values of m and n other than 1. Further, the ultimate strength has been estimated by investigating a last ply failure condition. Two different types of composite layup are considered [9]:

- Case A, a triaxial layup: $\left[-45 / +45 / 0_4 / +45 / -45 / 0_4 / -45 / +45 / 0_3\right]_S$
- Case B, a quasi-isotropic, quadriaxial layup: $\left[0 / +45 / 90 / -45\right]_{X,S}$

For the triaxial layups (case A), the required b/t values are achieved by scaling the thickness of each individual ply [9]. For the quadriaxial layups (case B), the thickness is increased by adding groups of plies (increasing X) to give the desired b/t values [9]. The

material properties and the plate thicknesses for cases A and B are given in Tables 1-3.

For the ply region degradation model (see Fig. 4), the size of regions 1, 3, 7 and 9 is 160 mm × 160 mm. Regions 2 and 8 are each 180 mm × 160 mm, while regions 4 and 6 is 160 mm × 180 mm. Finally, region 5 has the size 180 mm × 180 mm.

Table 1
Material properties (strengths and moduli).

Property	Value	Units
E_1	49627	MPa
E_2	15430	MPa
ν_{12}	0.272	-
G_{12}	4800	MPa
G_{13}	4800	MPa
G_{23}	4800	MPa
X_t	968	MPa
X_c	915	MPa
Y_t	24	MPa
Y_c	118	MPa
S_{12}	65	MPa

Table 2
Plate thicknesses and ply thicknesses for case A.

b/t	t (mm)	t_0 (mm)	$t_{\pm 45}$ (mm)
10	50.00	1.95	0.59
20	25.00	0.97	0.30
50	10.00	0.39	0.12

Table 3
Plate thicknesses and ply thicknesses for case B.

b/t	t (mm)	X	t_0, $t_{\pm 45}$, t_{90} (mm)
62.50	8.00	1	1.00
20.83	24.00	3	1.00
10.42	48.00	6	1.00

7.2 Step size and total number of degrees of freedom

The physical step size along the equilibrium path is dependent on the chosen propagation parameter value $\Delta\eta$ and the chosen size of the load interval (the applied reference load value N_x). Further, as an option, the reference load N_x could be determined by the elastic critical load. In Fig. 5, the influence of the step size $\Delta\eta$ on the accuracy of ultimate strength estimations is presented. The total number of increments used in a calculation is given as the inverse of the propagation parameter, $1/\Delta\eta$. Further, the ultimate strengths are plotted relative to a ultimate strength $\sigma_{\max,100}$ estimated with a small value of $\Delta\eta = 0.01$ ($1/\Delta\eta = 100$).

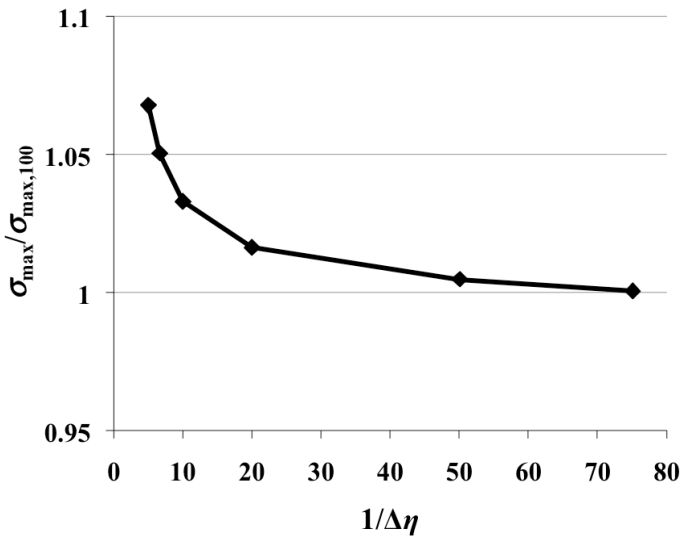

Fig. 5. The ultimate strength relation is plotted against $1/\Delta\eta$ for case A with t = 24.94 mm and 1% imperfection using CPDM.

In order to reduce the computation time, larger propagation parameter values may be considered. The calculated strength using $\Delta\eta = 0.05$ is about 1.5% larger than $\sigma_{max,100}$, but is time consuming to run. To achieve reasonable results within a reasonable computational time, $\Delta\eta = 0.10$ has been chosen for further calculations for all cases even the deviation is about 3% compared to $\sigma_{max,100}$. For case B, t = 8 mm, the ultimate strengths have been predicted using $\Delta\eta = 0.01$ due to few plies and small thickness.

The total number of degrees of freedom is defined by the total number of terms given in equations (4) and is another factor that will influence the accuracy of ultimate strength predictions. A convergence test has been performed for some of the cases using both degradation models and they are presented in Tables A.1-A.3 in Appendix A. In the tables, for different imperfections, plate thicknesses and the total number of degrees of freedom included, the strength estimations using the present method have been compared to the results provided by Misirlis [9]. Again, the computation time plays an important role for choosing the applicable total number of degrees of freedom. In general, more degrees of freedom that only gives less than 1% improvement has been discarded.

For case A using CPDM, based on Table A.1:

- t = 10.02 mm and all imperfections, implemented with 407 degrees of freedom.
- t = 24.92 mm and all imperfections, implemented with 127 degrees of freedom.
- t = 49.98 mm and all imperfections, implemented with 127 degrees of freedom.

For case B using CPDM, based on Table A.2:

- t = 10.02 mm and all imperfections, implemented with 407 degrees of freedom.
- t = 24.92 mm and all imperfections, implemented with 247 degrees of freedom.

- t = 49.98 mm with 0.1% and 1% imperfections, implemented with 127 degrees of freedom. 3% imperfection has been implemented with 247 degrees of freedom.

For case A using PRDM, based on Table A.3:

- t = 10.02 mm and all imperfections, implemented with 407 degrees of freedom. Not applicable with more degrees of freedom due to time consuming calculation. Besides it is believed that 407 degrees of freedom will give a good approach of deformations.
- t = 24.92 mm with 0.1% imperfection, implemented with 127 degrees of freedom. 1% and 3% imperfections are implemented with 247 degrees of freedom.
- t = 49.98 mm and all imperfections, implemented with 127 degrees of freedom.

For case B using PRDM, there is no convergence test performed. But according to Table A.2 (CPDM), the following is believed to provide a satisfactory approach of deformations:

- t = 8 mm and all imperfections, implemented with 407 degrees of freedom.
- t = 24 mm and all imperfections, implemented with 247 degrees of freedom.
- t = 48 mm and all imperfections, implemented with 247 degrees of freedom.

7.3 Load-displacement response without material degradation

The load-deflection response without material degradation for an imperfect plate using the present method implemented in Fortran is presented below. According to Figs. 6-7, to give a reasonable load-deflection responses for case A (t = 10.02 mm and 1% imperfection) and case B (t = 24 mm and 1% imperfection), respectively, at least 127 degrees of freedom will be needed.

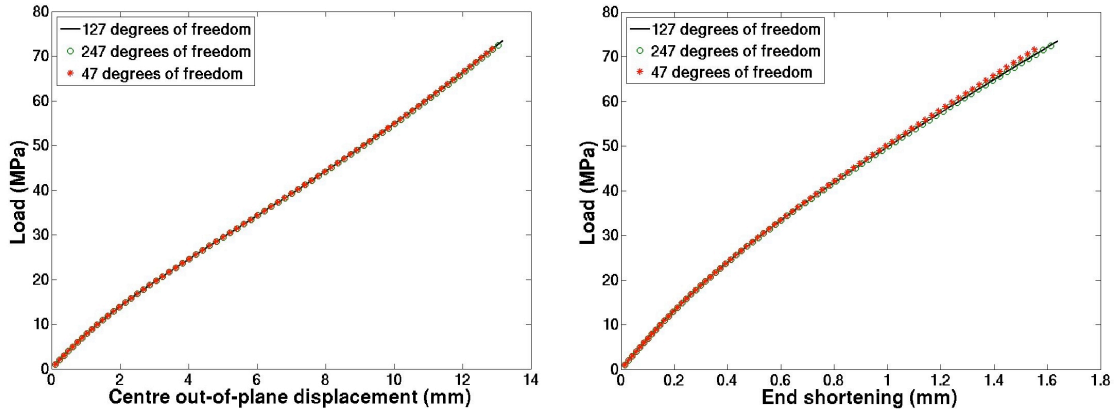

Fig. 6. Load vs. centre out-of-plane displacement and load vs. end shortening for case A, t = 10.02 mm and 1% imperfection. The stars show the results for 47 degrees of freedom, while the line shows for 127 degrees of freedom. The circles provide the results given by 247 degrees of freedom.

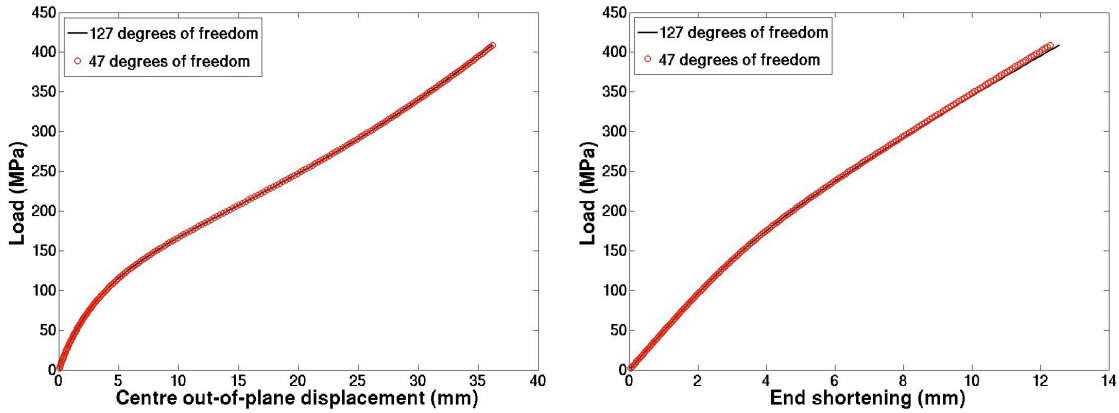

Fig. 7. Load vs. centre out-of-plane displacement and load vs. end shortening for case B, t = 24 mm and 1% imperfection. The circles show the results for 47 degrees of freedom, while the line shows for 127 degrees of freedom.

Further, the load-displacement responses obtained by the present method (implemented with 127 degrees of freedom) have been compared with finite element analyses using ANSYS with element type SHELL281 and element size 25 × 25 mm^2 for a range of plate thicknesses and imperfections (Figs. 8-13).

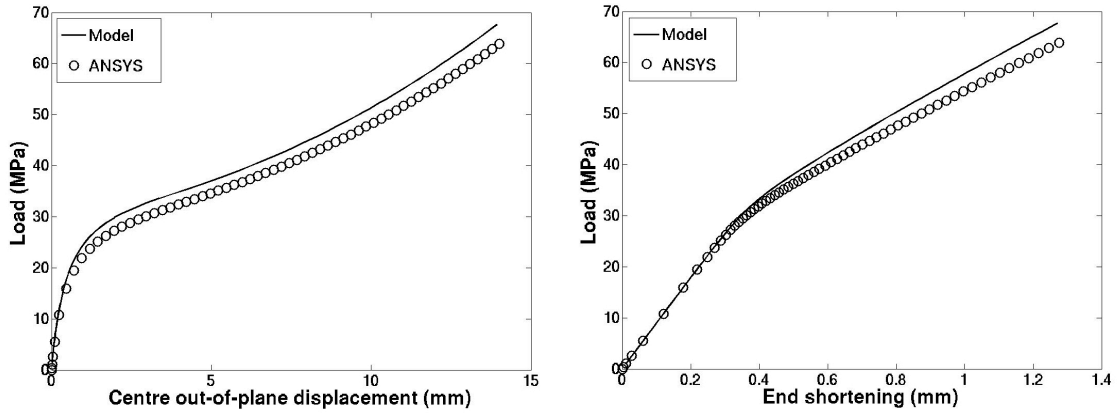

Fig. 8. Load vs. centre out-of-plane displacement and load vs. end shortening for case A, t = 10.02 mm and 0.1% imperfection. The line shows the results from the present method and the circles are the results form ANSYS.

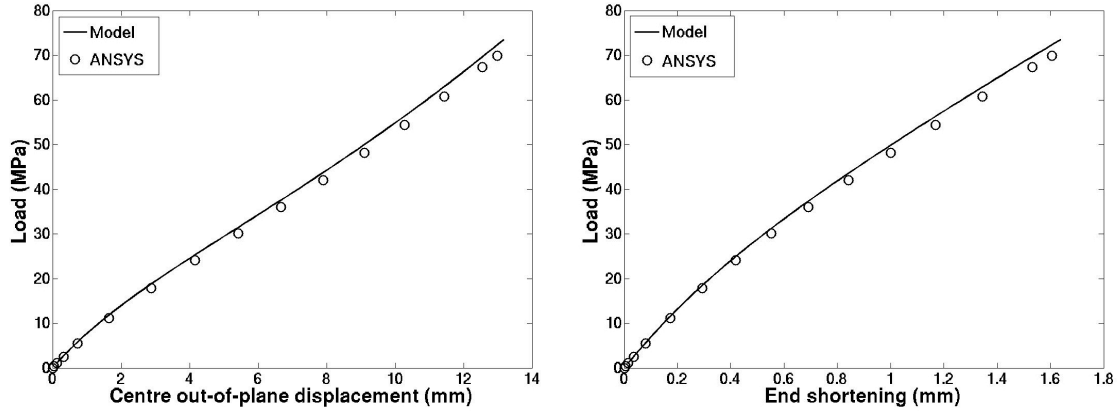

Fig. 9. Load vs. centre out-of-plane displacement and load vs. end shortening for case A, t = 10.02 mm and 1% imperfection. The line shows the results from the present method and the circles are the results from ANSYS.

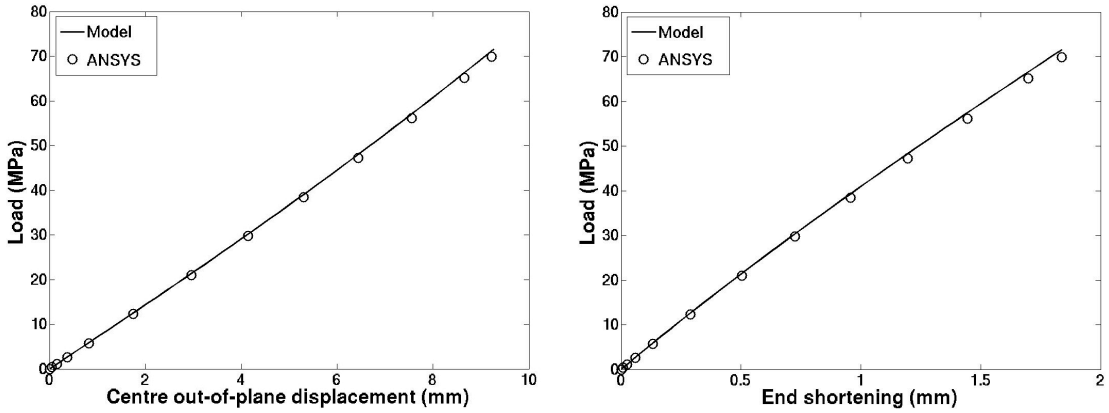

Fig. 10. Load vs. centre out-of-plane displacement and load vs. end shortening for case A, t = 10.02 mm and 3% imperfection. The line shows the results from the present method and the circles are the results from ANSYS.

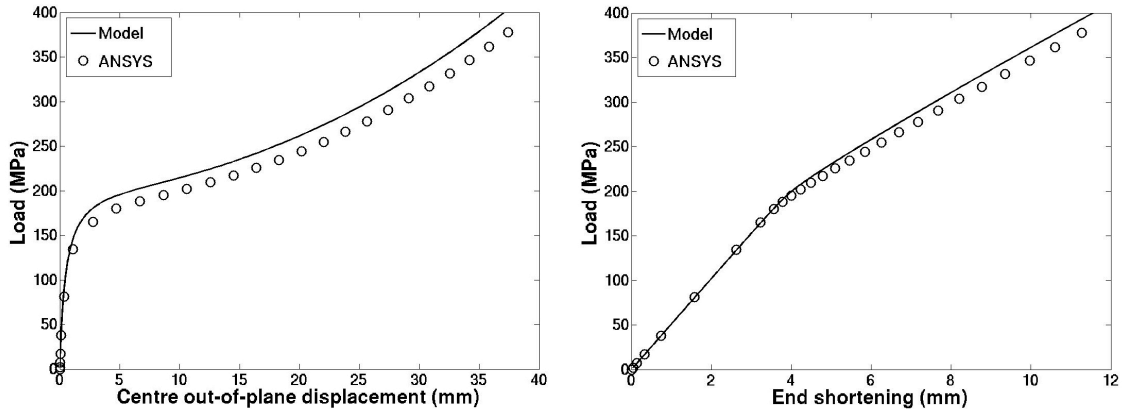

Fig. 11. Load vs. centre out-of-plane displacement and load vs. end shortening for case B, t = 24 mm and 0.1% imperfection. The line shows the results from the present method and the circles are the results from ANSYS.

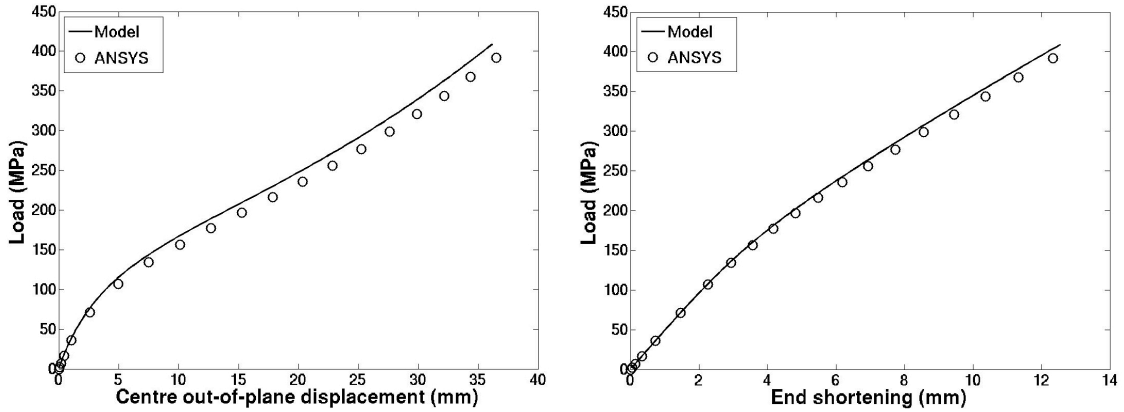

Fig. 12. Load vs. centre out-of-plane displacement and load vs. end shortening for case B, t = 24 mm and 1% imperfection. The line shows the results from the present method and the circles are the results from ANSYS.

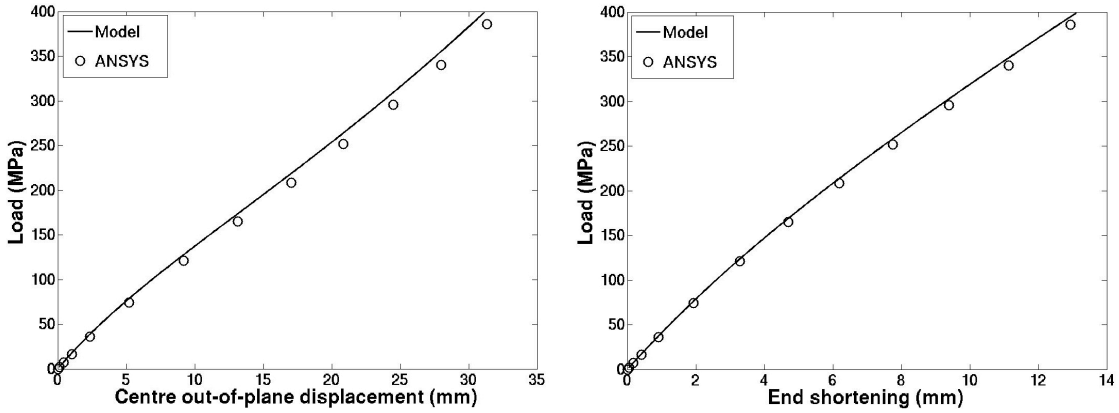

Fig. 13. Load vs. centre out-of-plane displacement and load vs. end shortening for case B, t = 24 mm and 3% imperfection. The line shows the results from the present method and the circles are the results from ANSYS.

From Figs. 8-13, the present method gives slightly greater plate stiffness than the ANSYS analyses, especially in the post-buckling area. Deviations are greatest for small imperfection, while good agreements are achieved for larger imperfections. The reason for this rather surprising trend is unclear at this stage of the work. Anyway, the small geometric imperfection investigated (0.1%) in the parametric study is quite unrealistic in the real world, and is intended as an academic imperfection.

7.4 Ultimate strength predictions using CPDM

Tables 4 and 5 show the results for case A and B, respectively, using the complete ply degradation model. For a given initial geometric imperfection amplitude, plate thickness (t) and total number of plies, the following are shown in these tables:

- At first ply failure (FPF), the calculated stress (σ_{FPF}) and location of first failure in terms of ply number and direction of that ply.
- The ultimate stress (σ_{max}) estimated by investigating a last ply failure condition ("LPF"). Also shown are the ply in which this last ply failure occurs (as ply number and direction) and the number of plies that have failed (both matrix and fibre) at this stage.

Further, in Tables 4 and 5, the results from the analysis are compared with those conducted by Misirlis (σ_{max} from [9]). The ratio of the ultimate strength from the present model to that found by Misilis are given in the last column (σ_{max} /σ_{max} from [9]). These are shown again in Figs. 14 and 15 for various values of the plate thickness t and imperfection amplitude.

Table 4
Complete ply degradation model: Case A (triaxial layup) with Hashin failure criterion.

Imp. % of *b*	*t* (mm)	No. of plies	FPF		"LPF"			σ_{max} from [9] (MPa)	$\frac{\sigma_{max}}{\sigma_{max}[9]}$
			σ_{FPF} (MPa)	Ply no. (direction)	σ_{max} (MPa)	No. of matrix (fibre) failed plies	Ply no. (direction)		
0.1	10.02	34	39.86	32 (0°)	94.94	34 (1)	34 (-45°)	130	0.73
0.1	24.94	34	172.00	32 (0°)	186.66	34 (1)	34 (-45°)	240	0.78
0.1	49.98	34	382.13	1 (-45°)	453.24	34 (1)	3 (0°)	570	0.80
1.0	10.02	34	31.64	32 (0°)	90.92	34 (1)	34 (-45°)	130	0.70
1.0	24.94	34	71.64	32 (0°)	171.40	34 (1)	34 (-45°)	235	0.73
1.0	49.98	34	149.55	32 (0°)	374.88	34 (1)	3 (0°)	435	0.86
3.0	10.02	34	22.96	32 (0°)	87.73	34 (1)	34 (-45°)	130	0.67
3.0	24.94	34	39.05	32 (0°)	149.98	34 (1)	34 (-45°)	218	0.69
3.0	49.98	34	64.26	32 (0°)	292.84	34 (1)	34 (-45°)	360	0.81

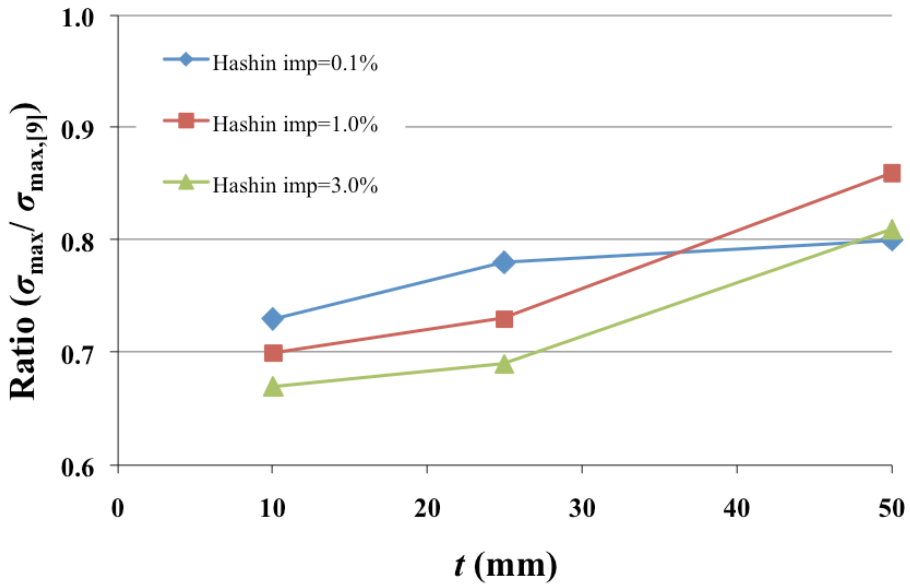

Fig. 14. Case A (triaxial layups) with complete ply degradation model: the ultimate strength from the present analyses are compared to those of Misirlis [9] for various plate thickness *t* and imperfection amplitude.

Table 5
Complete ply degradation model: Case B (quadriaxial layup) with Hashin failure criterion.

Imp. % of b	t (mm)	No. of plies	FPF		"LPF"			σ_{max} from [9] (MPa)	$\frac{\sigma_{max}}{\sigma_{max}[9]}$
			σ_{FPF} (MPa)	Ply no. (direction)	σ_{max} (MPa)	No. of matrix (fibre) failed plies	Ply no. (direction)		
0.1	8.00	8	29.08	8 (0°)	89.85	8 (1)	7 (45°)	105	0.86
0.1	24.00	24	170.92	24 (0°)	177.66	24 (1)	1 (0°)	215	0.83
0.1	48.00	48	204.13	3 (90°)	301.97	36 (1*)	1 (0°)	340	0.89
1.0	8.00	8	27.38	8 (0°)	91.51	8 (2)	2 (45°)	107	0.86
1.0	24.00	24	69.49	24 (0°)	171.48	24 (1)	23 (45°)	210	0.82
1.0	48.00	48	144.77	48 (0°)	250.92	42 (1*)	1 (0°)	302	0.83
3.0	8.00	8	26.08	8 (0°)	94.11	8 (1)	7 (45°)	115	0.82
3.0	24.00	24	35.62	24 (0°)	162.77	24 (2)	2 (45°)	205	0.79
3.0	48.00	48	61.70	48 (0°)	211.24	48 (1)	1 (0°)	260	0.81

*In these plies fibre failure occurred without matrix failure.

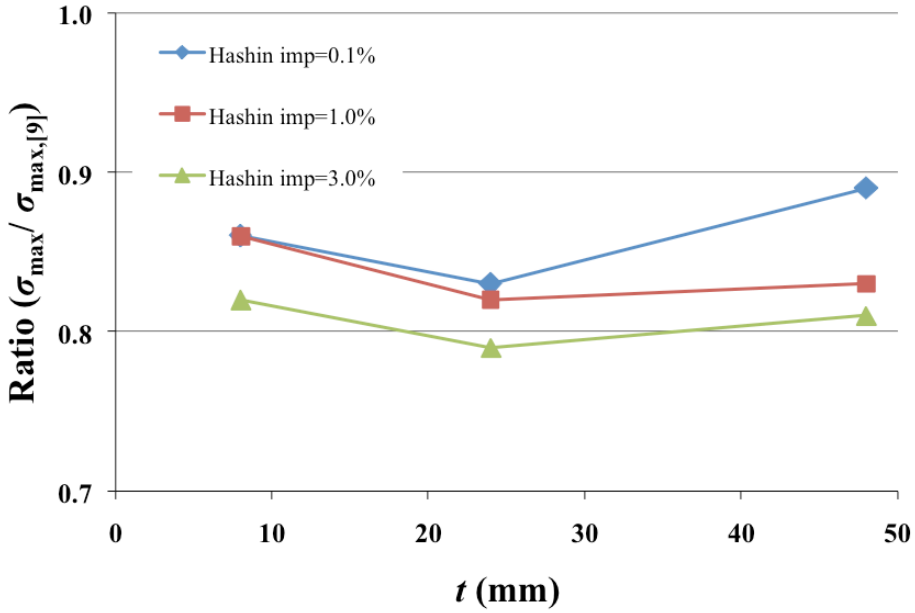

Fig. 15. Case B (quadriaxial layup) with complete ply degradation model: the ultimate strengths from the present analyses are compared to those of Misirlis [9] for various plate thickness t and imperfection amplitude.

7.5 Ultimate strength predictions using PRDM

Table 6 gives the results for the case A layups, using the ply region degradation model. Table 7 shows the corresponding results for the case B layups. For a given initial geometric imperfection amplitude, in addition to the number of plies, these tables also provide the total number of regions for each plate thickness. For the ultimate stress (σ_{max}), it is interesting to show the number of matrix failed regions and fibre failed

regions. Further, the results from the analysis are compared with those conducted by Misirlis (σ_{max} from [9]). The ratio of the ultimate strength from the present model to that found by Misirlis are given in the last column (σ_{max} /σ_{max} from [9]). These are again shown in Figs. 16 and 17 for various values of the plate thickness t and imperfection amplitude.

Table 6
Ply region degradation model: Case A (triaxial layup) with Hashin failure criterion.

Imp. % of b	t (mm)	No. of plies (no. of regions)	FPF		"LPF"			σ_{max} from [9] (MPa)	$\frac{\sigma_{max}}{\sigma_{max}[9]}$
			σ_{FPF} (MPa)	Ply no. (direction)	σ_{max} (MPa)	No. of matrix failed regions	No. of fibre failed regions		
0.1	10.02	34 (306)	39.86	32 (0°)	106.24	277	9	130	0.82
0.1	24.94	34 (306)	172.00	32 (0°)	186.68	293	2	240	0.78
0.1	49.98	34 (306)	382.13	1 (-45°)	453.24	306	1	570	0.80
1.0	10.02	34 (306)	31.64	32 (0°)	99.57	302	18	130	0.77
1.0	24.94	34 (306)	71.39	32 (0°)	175.34	276	12	235	0.75
1.0	49.98	34 (306)	149.55	32 (0°)	375.89	301	1*	435	0.86
3.0	10.02	34 (306)	22.96	32 (0°)	96.03	303	18	130	0.74
3.0	24.94	34 (306)	38.92	32 (0°)	155.30	276	10	218	0.71
3.0	49.98	34 (306)	64.26	32 (0°)	299.73	301	14	360	0.83

*In these regions fibre failure occurred without matrix failure.

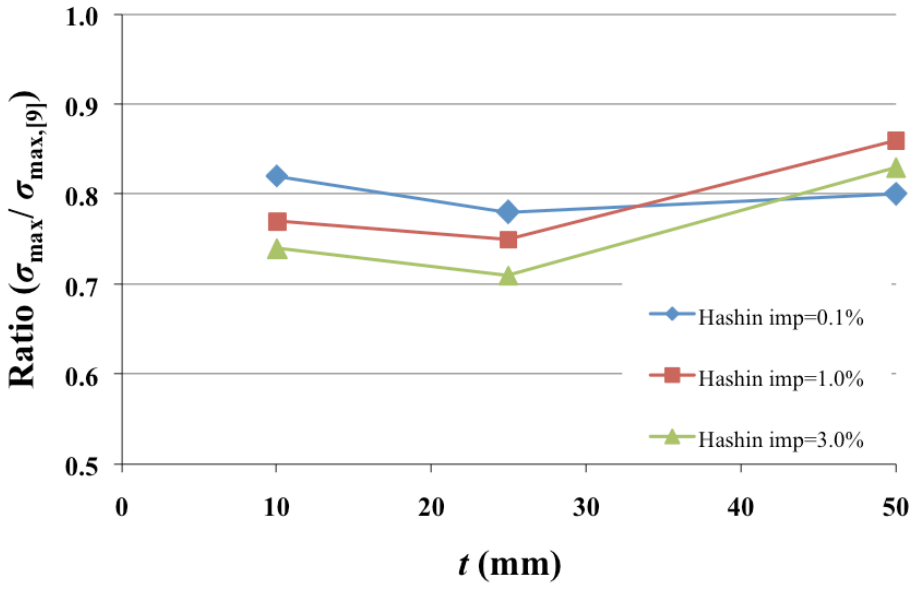

Fig. 16. Case A (triaxial layups) with ply region degradation model: the ultimate strength from the present analyses are compared to those of Misirlis [9] for various plate thickness t and imperfection amplitude.

Table 7
Ply region degradation model: Case B (quadriaxial layup) with Hashin failure criterion.

Imp. % of *b*	*t* (mm)	No. of plies (no. of regions)	FPF		"LPF"			σ_{max} from [9] (MPa)	$\frac{\sigma_{max}}{\sigma_{max}[9]}$
			σ_{FPF} (MPa)	Ply no. (direction)	σ_{max} (MPa)	No. of matrix failed regions	No. of fibre failed regions		
0.1	8.00	8 (72)	29.08	8 (0°)	101.71	57	3	105	0.97
0.1	24.00	24 (216)	170.92	24 (0°)	178.32	209	1	215	0.83
0.1	48.00	48 (432)	204.13	3 (90°)	301.97	324	1*	340	0.89
1.0	8.00	8 (72)	27.38	8 (0°)	101.54	56	4	107	0.95
1.0	24.00	24 (216)	69.49	24 (0°)	177.05	208	4	210	0.84
1.0	48.00	48 (432)	144.77	48 (0°)	250.92	378	1*	302	0.83
3.0	8.00	8 (72)	26.08	8 (0°)	101.86	54	4	115	0.89
3.0	24.00	24 (216)	35.62	24 (0°)	170.62	202	6	205	0.83
3.0	48.00	48 (432)	61.70	48 (0°)	209.70	392	1*	260	0.81

*In these regions fibre failure occurred without matrix failure.

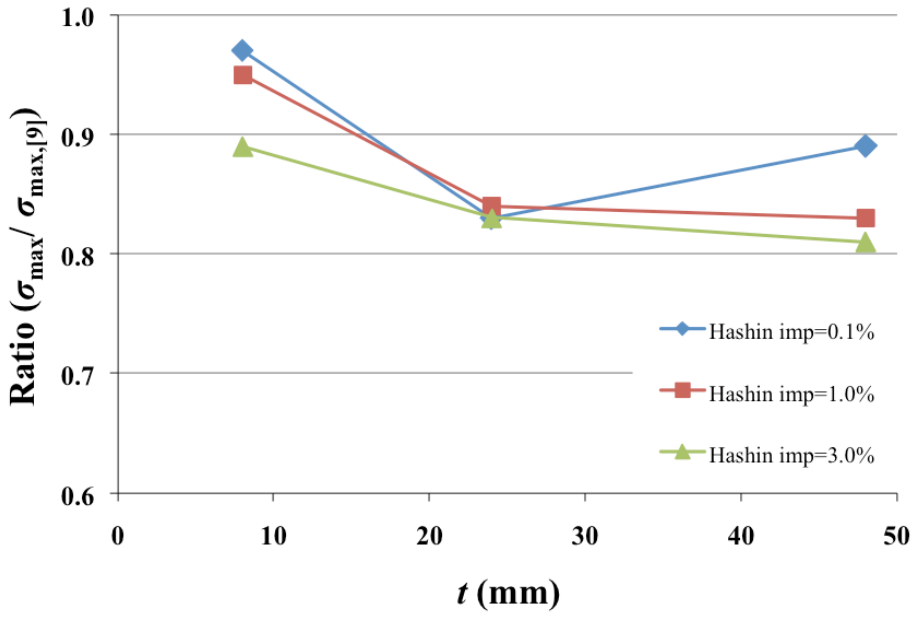

Fig. 17. Case B (quadriaxial layup) with ply region degradation model: the ultimate strengths from the present analyses are compared to those of Misirlis [9] for various plate thickness *t* and imperfection amplitude.

Further, in Fig. 18, the applied load is plotted against displacement in the centre and the end shortening response for case A with $t = 10.02$ mm and *imp.* = 0.1%. The corresponding results are presented in Fig. 19 for case A with $t = 49.98$ mm and *imp.* = 1%. For case B with $t = 24$ mm and *imp.* = 3%, the similar results are shown in Fig. 20.

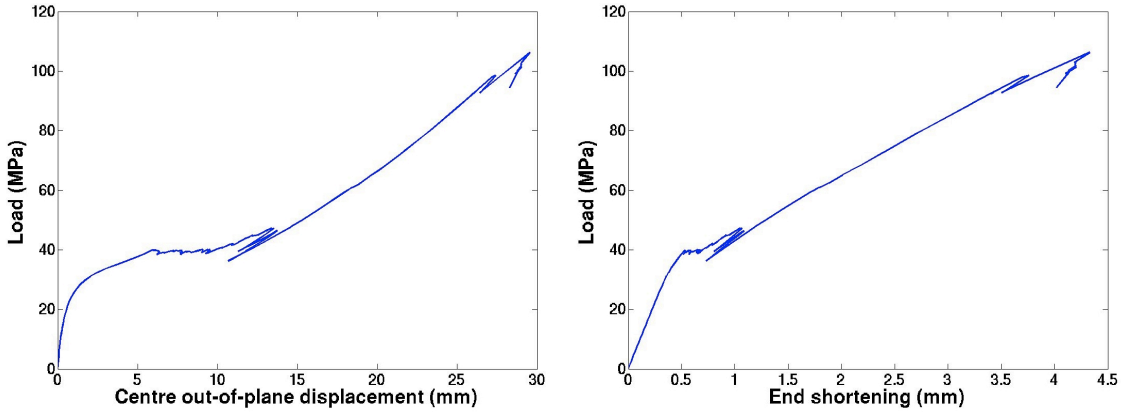

Fig. 18. Case A (triaxial layup), for t = 10.02 mm and 0.1% imperfection amplitude, using ply region degradation model. Load vs. centre out-of-plane displacement and end shortening.

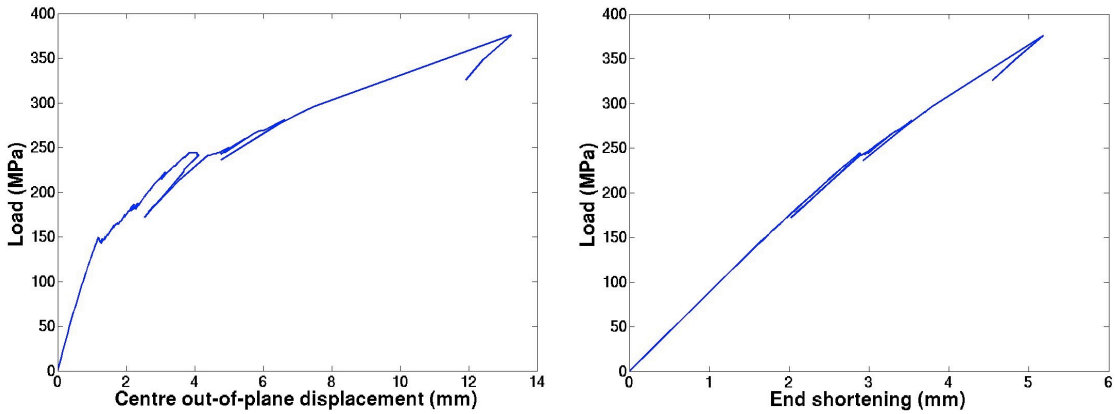

Fig. 19. Case A (triaxial layup), for t = 49.98 mm and 1% imperfection amplitude, using ply region degradation model. Load vs. centre out-of-plane displacement and end shortening.

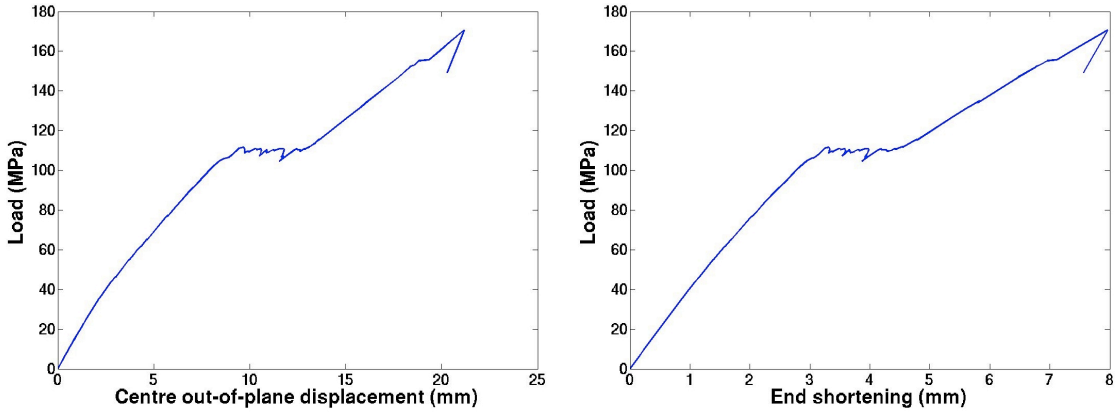

Fig. 20. Case B (quadriaxial layup), for t = 24 mm and 3% imperfection amplitude, using ply region degradation model. Load vs. centre out-of-plane displacement and end shortening.

8 DISCUSSION OF RESULTS

8.1 Results using CPDM

For case A – first ply failure:

- Failure usually occurs in the outer plies, most of all those of the convex side of the plate. The outermost 0° plies always fail (matrix) first for all cases except for the thickest plate (t = 49.98 mm) with 0.1% imperfection. For that case, the matrix failure occurred in the outermost -45° ply.

For case A – "last ply failure":

- For all cases, all plies have to fail in matrix and the ultimate strength is reached at the first incidence of fibre failure.
- Compared to Misirlis's FE analysis, the deviations are in the range of 14-33%.

For case B – first ply failure:

- Failure usually occurs in the outer plies, primarily those at the convex side of the plate. The outermost 0° plies always fail (matrix) first for all cases except for the thickest plate (t = 48 mm) with 0.1% imperfection. For that case, the matrix failure occurred in the 90° ply.

For case B – "last ply failure":

- For thin (t = 8 mm) and moderately thick plates (t = 24 mm), all plies have to experience matrix failure. The ultimate strength is attained at the first, sometimes the second incidence of fibre failure.
- For the thick plate (t = 48 mm) with 3% imperfection, all plies experienced matrix failure and the ultimate strength is reached at the first occurrence of fibre failure.
- For the thick plate with 0.1% imperfection, all ±45° plies have to fail in matrix before the occurrence of the ultimate strength, which is at the first incidence of fibre failure in a 0° ply without matrix failure.
- For the thick plate with 1% imperfection, in addition to all ±45° plies, some of the 0° plies have to fail in matrix before the occurrence of the ultimate strength, which is at the first fibre failure in a 0° ply without matrix failure.
- Compared to Misirlis's FE analysis, the deviations are in the range of 11-21%.

In general, the 0° and 90° plies often fail first in the centre of the plate, while the ±45° plies fail at the corners.

8.2 Results using PRDM

Compared to CPDM, the ultimate strength predictions using PRDM need more degrees of freedom for some of the cases investigated. There are no significant differences for first ply failure compared with CPDM, i.e. more degrees of freedom implemented in PRDM will only cause deviations in negligible decimals.

For case A – "last ply failure":

- For all cases, many regions have to fail in matrix before the ultimate strength is attained at the fibre failure. For the thick plate (t = 49.98 mm) with 1% imperfection, the ultimate strength is reached at the first incidence of fibre failure in a region without matrix failure.
- Compared to Misirlis's FE analysis, the deviations are in the range of 14-29%.

For case B – "last ply failure":

- For all cases, many regions have to experience matrix failure before the ultimate strength is attained at fibre failure. For thick plates (t = 48 mm), fibre failure occurred in regions without matrix failure.
- Compared to Misirlis's FE analysis, the deviations are in the range of 3-19%.

Further, the central out-of-plane response and the end shortening of a thin plate in case A (t = 10.02 mm and *imp.* = 0.1%) are provided in Fig. 18. The ultimate load is reached at 106.24 MPa and resulted in a central displacement of 29.54 mm and an end shortening of 4.33 mm.

The centre out-of-plane displacement and the end shortening of a thick plate in case A (t = 49.98 mm and *imp.* = 1%) are given in Fig. 19. The central out-of-plane displacement and the end shortening are 13.25 mm and 5.18 mm, respectively, at the ultimate load of 375.89 MPa.

For a moderately thick plate in case B (t = 24 mm and *imp.* = 3%), Fig. 20 shows the out-of-plane displacement in the centre and the end shortening response. The ultimate load is achieved at 170.62 MPa with the corresponding lateral displacement of 21.17 mm in the centre and end shortening of 7.96 mm.

8.3 Comparison between results using CPDM, PRDM and Misirlis's model

From the analyses with CPDM, the predicted ultimate stresses are 11% – 33% smaller than those of Misirlis. The most significant differences are observed in the triaxial layup configuration, case A. The greatest deviations are found for thin plates (t = 10.02 mm), being in the range of 27% – 33%. For moderately thick (t = 24.94 mm) and thick plates (t = 49.98 mm), they are in the range of 22% – 31% and 14% – 20%, respectively. However, for the balanced layup configuration, case B, the ultimate strength predictions using CPDM produced a more stable deviation in the range of 11% – 21%. The analyses with PRDM provide better estimates for some of the cases. Especially for thin plates, which are more sensitive to material degradation, PRDM gives significantly better results. The greatest improvements (7% – 11%) between the results using CPDM and PRDM are found for the quadri-axial layup configuration, case B. For case A, the improvements are about 7% – 9%. The improvements achieved are either negligible or quite small for moderately thick and thick plates for both cases (0% – 4%).

The current analyses have been implemented with an instantaneous material degradation assumption when failure occurs. Thus, it will result in too much degradation of the plate stiffness. This is believed to be the main reason of the underestimations of ultimate strength since the fully nonlinear FE analyses use a linear material degradation in their progressive failure model.

9 CONCLUSION

The ultimate strength analysis of simply supported square plates subjected to in-plane compressive load has been performed using a semi-analytical method. Based on large deflection theory and first order shear deformation theory in combination with two degradation approaches, the present model is able to take account of post-buckling deformations, out-of-plane deformations and geometric imperfections. The results have been compared with an advanced analysis conducted by Misirlis using fully non-linear FE analysis. In the first approach, called complete ply degradation model (CPDM), fulfilment of the failure criterion at any position in a ply leads to instantaneous degradation of corresponding stiffness properties throughout that ply. In the slightly more detailed approach, called ply region degradation model (PRDM), the plate is divided into nine regions and the stiffness degradation is limited to the affected regions of a failed ply. Both approaches are shown to give reasonable, but still conservative estimates of ultimate loads. For thinner plates, the analyses with PRDM provide significantly better predictions, while there is no obvious improvement between the results using CPDM and PRDM for thicker plates. Underestimations by using the present method compared with the nonlinear FE analysis is due to a linear degradation of the material properties in Misirlis's progressive failure model, while the current analyses assumed a instantaneous degradation of the material properties. To improve the results and give a more accurate estimation of the ultimate stresses, future extension of the work will implement a linear degradation model combined with PRDM.

REFERENCES

[1] E. Steen. Application of the perturbation method to plate buckling problem. Research Report in Mechanics, No. 98-1, Mechanics Division, Dept. of Mathematics, University of Oslo, Norway, 1998.

[2] L. Brubak, J. Hellesland and Eivind Steen. Semi-Analytical Buckling Strength Analysis of Plates with Arbitrary Stiffener Arrangements, Journal of Constructional Steel Research (2007), Vol. 63, No. 4, pp. 532-543.

[3] L. Brubak and J. Hellesland. Approximate Buckling Strength Analysis of Arbitrarily Stiffened, Stepped Plates, Engineering Structures (2007), Vol. 29, No. 9, pp. 2321-2333.

[4] L. Brubak and J. Hellesland. Semi-Analytical Postbuckling and Strength Analysis of Arbitrarily Stiffened Plates in Local and Global Bending, Thin-Walled Structures (2007), Vol. 45, No. 6, pp. 620-633.

[5] L. Brubak and J. Hellesland. Strength Criteria in Semi-Analytical, Large Deflection Analysis of Stiffened Plates in Local and Global Bending, Thin-walled Structures

(2008), Vol. 46, No. 12, pp. 1382-1390.

[6] L. Brubak and J. Hellesland. Semi-Analytical Postbuckling Analysis of Stiffened Imperfect Plates with a Free or Stiffened Edge, Computers and Structures (2011), Vol. 89, No. 17-18, pp. 1574-1585.

[7] Q. J. Yang, B. Hayman and H. Osnes. Trials with a simplified method for buckling and ultimate strength analysis of composite plates. Research Report in Mechanics, No. 1, Mechanics Division, Dept. of Mathematics, University of Oslo, Norway, 2012.

[8] Z. Hashin and A. Rotem. A Fatigue Failure Criterion for Fiber Reinforced Materials, Journal of Composite Materials (1973), Vol. 7, pp 448-464.

[9] B. Hayman, C. Berggreen, C. Lundsgaard-Larsen, A. Delarche, H. Toftegaard, R.S. Dow, J. Downes, K. Misirlis, N. Tsouvalis and C.Douka. Studies of the Buckling of Composite Plates in Compression, Ships and Offshore Structures (2011), Vol. 6, Nos. 1-2, pp. 81-92.

[10] J. N. Reddy. Mechanics of Laminated Composite Plates and Shells, CRC Press, USA, 2nd Edition, 2004.

[11] K. Marguerre. Zur theorie der gekrümmten platte grosser formänderung, Proceedings of The 5th International Congress for Applied Mechanics, 1938; 93-101.

[12] Bhagwan D. Agarwal, Lawrence J. Broutman and K. Chandrashekhara. Analysis and Performance of Fiber Composites, Wiley, USA, 3rd Edition, 2006.

[13] E. Byklum. Ultimate strength analysis of stiffened steel and aluminium panels using semi-analytical methods, Dr. Ing. thesis, Norwegian University of Science and Technology, Trondheim, Norway, 2002.

[14] E. Riks. An incremental approach to the solution of snapping and buckling problems, International Journal of Solids and Structures, 1979; 15: 529-551.

[15] Offshore Standard DNV-OS-C501 Composite Components. Det Norske Veritas, Norway, 2003.

[16] A. Matzenmiller, J. Lubliner and R. L. Taylor. A Constitutive Model for Anisotropic Damage in Fiber-composites, Mechanics of Materials 20 (1995) 125-152.

APPENDIX A: TABULATED RESULTS FOR SECTION 7.2

Table A.1
The ultimate strengths for case A using CPDM.

Imperfection in % of b	Plate thickness (mm)	Total number of degrees of freedom	Ultimate strength, σ_{max} (MPa)	Ultimate strength, σ_{max} (MPa) from [9]	$\sigma_{max}/\sigma_{max,[9]}$
0.1	10.02	47 ($N = M = 3$)	133.85	130	1.03
		127 ($N = M = 5$)	105.76	130	0.81
		249 ($N = M = 7$)	97.50	130	0.75
		407 ($N = M = 9$)	94.94	130	0.73
		607 ($N = M = 11$)	94.22	130	0.72
3.0	10.02	127 ($N = M = 5$)	101.89	130	0.78
		249 ($N = M = 7$)	91.40	130	0.70
		407 ($N = M = 9$)	87.73	130	0.67
		607 ($N = M = 11$)	86.65	130	0.67
1.0	24.94	47 ($N = M = 3$)	177.17	235	0.75
		127 ($N = M = 5$)	171.40	235	0.73
		249 ($N = M = 7$)	170.65	235	0.73
		407 ($N = M = 9$)	170.16	235	0.72
3.0	24.94	47 ($N = M = 3$)	159.51	218	0.73
		127 ($N = M = 5$)	149.98	218	0.69
		249 ($N = M = 7$)	148.49	218	0.68
1.0	49.98	47 ($N = M = 3$)	376.88	435	0.87
		127 ($N = M = 5$)	374.88	435	0.86

Table A.2
The ultimate strengths for case B using CPDM.

Imperfection in % of b	Plate thickness (mm)	Total number of degrees of freedom	Ultimate strength, σ_{max} (MPa)	Ultimate strength, σ_{max} (MPa) from [9]	$\sigma_{max}/\sigma_{max,[9]}$
1.0	8	127 ($N = M = 5$)	111.27	107	1.04
		249 ($N = M = 7$)	96.75	107	0.90
		407 ($N = M = 9$)	91.51	107	0.86
		607 ($N = M = 11$)	90.38	107	0.84
1.0	24	47 ($N = M = 3$)	175.64	210	0.84
		127 ($N = M = 5$)	174.05	210	0.83
		249 ($N = M = 7$)	171.48	210	0.82
		407 ($N = M = 9$)	169.42	210	0.81
0.1	48	127 ($N = M = 5$)	301.97	340	0.89
		249 ($N = M = 7$)	301.97	340	0.89
3.0	48	47 ($N = M = 3$)	212.28	260	0.82
		127 ($N = M = 5$)	210.72	260	0.81
		249 ($N = M = 7$)	211.24	260	0.81

Table A.3
The ultimate strengths for case A using PRDM.

Imperfection in % of b	Plate thickness (mm)	Total number of degrees of freedom	Ultimate strength, σ_{max} (MPa)	Ultimate strength, σ_{max} (MPa) from [9]	$\sigma_{max}/\sigma_{max,[9]}$
3.0	24.94	127 ($N = M = 5$)	162.27	218	0.74
		249 ($N = M = 7$)	155.30	218	0.71
		407 ($N = M = 9$)	154.80	218	0.71
3.0	49.98	127 ($N = M = 5$)	299.73	360	0.83
		249 ($N = M = 7$)	302.73	360	0.84